Physicochemical Aspects of Novel Surfactantless, Self-Templated Mesoporous SnO_2 Thin Films

Celso Velásquez,[†,§] Fernando Rojas,[†] J. Marcos Esparza,[†] Armando Ortiz,[‡] and Antonio Campero*[,†]

Departamento de Química, Universidad Autónoma Metropolitana−Iztapalapa, P.O. Box 55-534, México, D.F. 09340, México, and Instituto de Investigaciones en Materiales, Universidad Nacional Autónoma de México, P.O. Box 70-360, México, D.F. 4510, México

Received: December 7, 2005; In Final Form: March 1, 2006

A novel method of synthesis consisting of the production of ordered arrangements of tubular pores distributed inside SnO_2 annealed thin films, which are prepared from a rotating disk process carried out at 2000−3500 rpm, is herein described. The main novelty is that no surfactant molecules are required in order to create these ordered pore structures; the templating entities are supramolecular assemblies of oligomeric chains formed during the extra-long aging allowed to the sol−gel processing of tin(IV) tetra-*tert*-amiloxide, Sn(OAm^t)$_4$, chelated with acetylacetone molecules. Low angle X-ray diffraction peaks of SnO_2 thin films calcined at 500 °C clearly certify the existence of ordered mesostructures when employing the right H_2O/Sn(OAm^t)$_4$ molar ratio during the SnO_2 sol−gel synthesis. The final SnO_2 ordered mesostructures are reminiscent of those linked to MCM-41 and SBA-15 substrates. Pore-size distribution analyses proceeding from N_2 sorption isotherms at 76 K on the SnO_2 thin films calcined at 500 °C unequivocally confirm the presence of tubular mesopores (mode pore sizes ranging from 5 to 7 nm). The thicknesses of the SnO_2 films range from 80 to 150 nm after performing a drying process at 100 °C and from 70 to 125 nm after calcining in air at 500 °C; these film thicknesses show, in general, decreasing trends when either the spinning rate or the H_2O/(Sn(OAm^t)$_4$ ratio is increased.

1. Introduction

SnO_2 has been prepared through a wide variety of processes such as spray pyroysis,[1] chemical vapor deposition,[2,3] sputtering,[4] and thermal evaporation,[5] among others. When SnO_2 is produced in the form of solid corpuscles endowed with voids of nanometric sizes, it can still exhibit some outstanding properties.

Many research efforts have been devoted to the effect of the amount of water employed during the synthesis of bulk silica gel[6,7] and its effects on some structural aspects of SnO_2 films.[8,9] Bradley and Holloway[10] observed, during a sol−gel SnO_2 synthesis, that the extent of oligomerization varies with the degree of hydrolysis (i.e., the number of water molecules that react per each tin atom). Gulliver et al.[11] noted that tin(IV) ethoxide can be efficiently hydrolyzed under basic conditions with an adequate amount of water to render spherical SnO_2 particles with sizes ranging from 7 to 25 nm.

Solid materials obtained by the sol−gel process are typically microporous or mesoporous substrates. Nowadays, some of the most impressive mesoporous materials correspond to those that are obtained from micelle templating techniques[12] and that render ordered pore arrangements of very uniform sizes, for example, MCM-41, SBA-15, or SBA-16. The interesting issue is that we are now convinced that pore arrangements of a similar sort can be synthesized by templating sol−gel surfactantless methods, such as that to be described in this work.

Here, we have prepared ordered, self-templating SnO_2 mesoporous thin films by reaching optimal hydrolysis and condensation extents of our Sn(IV) tetra-*tert*-amiloxide precursory molecules. Therefore, we have investigated one of the most important parameters of this synthesis: the amount of water employed for the sol−gel hydrolysis and condensation reactions in order to achieve uniform mesoporous thin solid films by a spinning technique. With the aim of accomplishing a total conversion of tin(IV) tetra-*tert*-amiloxide into SnO_2, through the hydrolysis and condensation reactions, 2 mol of water are required per each mole of Sn(IV) tetra-*tert*-amiloxide reactant. However, an excess of water is still required in order to reach an adequate conversion as well as appropriate textural properties; consequently, the effects of surplus H_2O amounts are also reported here.

In this work, we have controlled the Sn(IV) tetra-*tert*-amiloxide reactivity by the addition of chelatant acetylacetone (acac) molecules in order to avoid a fast hydrolysis reaction once water is added to the reactive alkoxide solution. This method of synthesis also allows the control of several other properties of SnO_2 thin films, such as thickness, electrical conductivity, optical transparency, and pore size.

This work is organized as follows. The experimental details for preparing ordered mesoporous SnO_2 thin films by a surfactantless method will be addressed first; afterward, the characterization techniques for measuring some of the most important physicochemical and textural properties of the above substrates will be described; finally, an overall assessment of the surfactantless synthesis and characterization of ordered, SnO_2 mesoporous films will be overtaken.

* To whom correspondence should be addressed. E-mail: acc35@xanum.uam.mx. Fax: +52 55 58044666. Phone: +52 55 58044677.
† Universidad Autónoma Metropolitana−Iztapalapa.
‡ Universidad Nacional Autónoma de México.
§ Present address: INAOE, CP 72840, Tonantzintla Pue., México.

10.1021/jp057141d CCC: $33.50
Published on Web 05/26/2006

TABLE 1: Volumes of Water (μL) That Are Mixed with 0.5 mL of Aged $Sn(OR)_4$ Solution[a]

$H_2O/Sn(OAm^t)_4$ molar ratio, R	2	3	4	5	6	7
H_2O (μL)	0	5.3	10.6	15.8	21.1	26.4

[a] Each preparation also includes 1 mL of 2-propanol and 10.5 μL of 0.1 M HCl.

2. Experimental Section

The reagents used for the synthesis of mesoporous tin oxide films were the following: Tin tetra-*tert*-amyloxide, $Sn(OAm^t)_4$, a very reactive alkoxide substance, was synthesized in our laboratory[13] by slightly modifying the procedure originally proposed by Thomas.[14] With regard to purity, a single narrow peak is seen in its corresponding ^{119m}Sn NMR spectrum. In turn, acetylacetone (Merck 99 wt %) was employed to chelate the alkoxide molecules and decrease its extreme reactivity. *tert*-Amyl alcohol, Am^tOH ($C_2H_5(CH_3)_2OH$, Aldrich 99 wt %), was chosen as a solvent of the above alkoxide in order to further control its reactivity through appropriate dilution. Reagent grade 0.1 M HCl (Fluka) was added to promote the growth of linear oligomeric aggregates and the eventual gelation of the tin alkoxide compound. Triply distilled water acted as the main reactant for inducing the pertinent hydrolysis−condensation reactions leading to gelation. Finally, 2-propanol (J.T. Baker 98 wt %) acted as a diluent in the reactant mixture.

2.1. SnO_2 Sol Preparation. A 2 mL portion (1.94×10^{-2} mol) of acac and 2 mL (4.7×10^{-3} mol) of $Sn(OAm^t)_4$ were mixed together in a round-bottomed flask and stirred vigorously for 10 min at room temperature, under an inert moisture-free N_2 atmosphere flowing continuously inside a hermetic glovebox. Afterward, a volume of 4 mL of 2-propanol (5.2×10^{-2} mol) was gradually added to the alkoxide mixture while continuing the stirring for a further 10 min. The resultant solution was aged for 3 months at room temperature. At the end of this time, an aliquot of 0.5 mL of the aged solution was mixed with 10.5 μL of 0.1 M HCl, followed by the gradual addition of 1 mL of 2-propanol. Soon after, water was added dropwise to the latter mixture in an appropriate amount to achieve a $H_2O/Sn(OAm^t)_4$ molar ratio, R, equal to 2 (i.e., 5.87×10^{-4} mol of H_2O/2.935×10^{-4} mol of $Sn(OAm^t)_4$. A series of SnO_2 sols was then prepared by choosing the proper amounts of distilled water to be mixed with the alkoxide reagent in order to create reactant mixtures having $R = 2$, 3, 4, 5, 6, and 7, as summarized in Table 1.

Each one of the above-described sol systems was then taken to refluxing conditions by raising the temperature of the bath enclosing the flask containing these gels up to 50 °C in 15 min. The reacting systems were next kept under refluxing and stirring conditions for a further 30 min. Finally, the sol dispersions were cooled until room temperature was attained.

2.2. SnO_2 Thin Film Formation. SnO_2 films were spread over square ($20 \times 20 \times 1.4$ mm^3) Pyrex glass plates. Prior to film creation, each glass plate was immersed for 5 min in a beaker placed inside an ultrasonic bath containing a solution of a cleaning agent. Subsequently, every glass plate was successively rinsed with abundant amounts of distilled water, acetone, distilled water, methanol, distilled water, and finally 2-propanol. Afterward, the cleaned glass plates were heat-treated at 80 °C for 10 min and then stored in a desiccator for later use.

The SnO_2 sols with $R = 2$, 3, and 4 were distributed uniformly on the surfaces of glass plates and then left to age for 30 min. A glass syringe, fitted with a 0.1 μm filter (Pall Gelman Lab.), constituted the dispensing system that allowed the application of an even amount of SnO_2 sol dispersion on the surface of each plate. Every glass substrate, once having a gelling SnO_2 sol deposited on the surface, was spun at 2000, 2500, 3000, and 3500 rpm, respectively; each coating operation was performed by means of a P6204 rotating instrument from Specialty Coating Systems Inc. In all cases, the spinning time was 60 s. The resultant coated glass substrates were then dried at 100 °C for 60 min on a hot plate in air. It was observed that SnO_2 sols with $R = 5$, 6, and 7 transformed spontaneously into gels, before completing the 30 min aging time, therefore preventing the preparation of any film related to the above compositions.

The thickness of each SnO_2 film was measured by means of a Dektak IIA surface profilometer.

2.3. Characterization Techniques. *XRD.* X-ray diffraction patterns of SnO_2 samples were obtained via a Siemens D-500 diffractometer coupled to a molybdenum anode tube. X-ray patterns were determined in the 2θ diffraction range extending from 0.4 to 10°, and intensity values were read at $\Delta(2\theta)$ intervals of 0.01° by employing a step time of 1.2 s.

TEM. Transmission electron microscopy studies were carried out with a JEM-2010F FASTEM electron microscope operating at 200 kV. The samples used for TEM inspection were first deposited on NaCl substrates and then spun up to 3500 rpm to obtain thin films, and afterward, they were calcined at 500 °C for 2 h. Finally, the calcined SnO_2 films were separated from their NaCl bases by dissolving these ones with distilled water. The separated SnO_2 films were next deposited on 300 mesh copper grids and subsequently dried in air before being analyzed by TEM.

N_2 Sorption. N_2 sorption isotherms at 76 K (at the 2200 m altitude of Mexico City) were measured with a Quantachrome 1-LC automatic instrument. The N_2 sorption measurements were performed exclusively on the SnO_2 films annealed at 500 °C. The SnO_2 films were introduced into the adsorption cell deposited on small square glass pieces of about 3 mm per side. These small pieces were cut from the original (larger) glass plates on which the SnO_2 films were deposited. It was found that 60 spin-coated glass plates rendered an appropriate SnO_2 film mass to perform sorption studies. Prior to the adsorption run, each SnO_2 film sample was outgassed overnight at 300 °C.

3. Results and Discussion

3.1. Preliminary Remarks. The balanced chemical equations for the chelation of $Sn(OAm^t)_4$ with acetylacetone can be visualized in Scheme 1. In the presence of an excess of acac, the original alkoxide precursor is transformed either into a linear dimer (first reaction in Scheme 1) if the excess of acac is slight or into a cyclic trimer (second reaction in Scheme 1) in the presence of a large excess of acac. In both cases, Sn−(OAm^t)−Sn bridges are formed. The acac molecule, acting as a bidentate chelating agent, then replaces the terminal *tert*-amyloxide (−OAm^t) ligands to give species **2** and **4** appearing in Scheme 1. The presence of the protecting acac bidentate ligands, as well as the rather low amount of water present, makes the hydrolysis−condensation reactions necessary to form the polymers constituting the gel network almost impossible. However, a certain weak amount of hydrolysis takes place, with the formation and release of *tert*-amyl alcohol molecules, which enhance slightly the condensation reactions, which take place during the 3 month delay time allowed for the aging of the sol, prior to the addition on purpose of water. Polymerization of these two last species, through the addition of water about 3

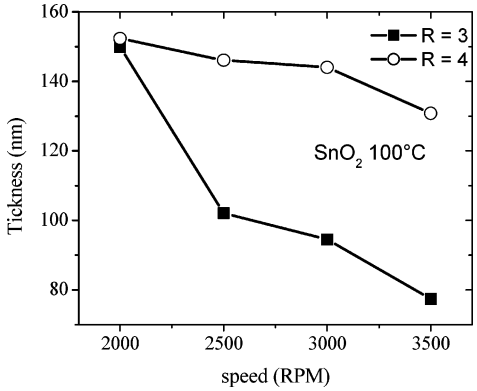

Figure 1. Thickness of SnO_2 xerogel films dried at 100 °C.

SCHEME 1: Chelation of acac to $Sn(OAm^t)_4$ and Subsequent Formation of Dimer and Trimer Species

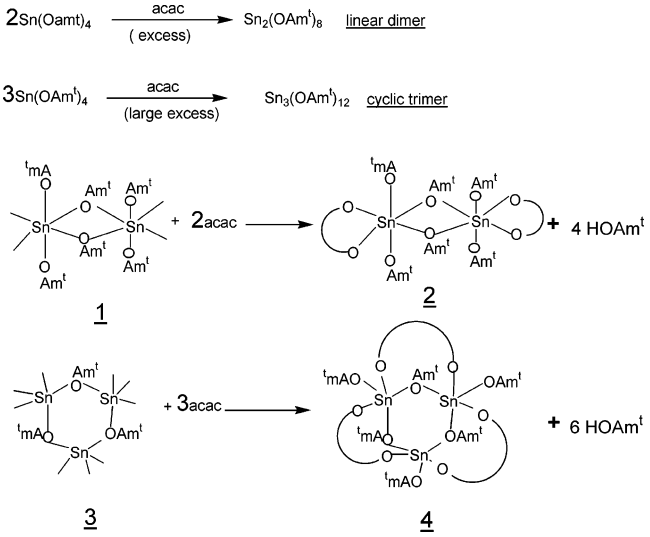

months after their formation, is quite likely responsible for the formation of the final mesoporous materials obtained in the absence of any surfactant agent.

The addition of acac as an inhibiting (i.e., chelating) agent[15] can modulate the extreme reactivity of $Sn(OAm^t)_4$. Once the alkoxide compound has been stabilized with acetylacetone, the proper amount of water can be added to the system to generate sols rather than gels. R values between 2 and 4 are needed to form stable sols; molar ratios higher than 4 (i.e., 5, 6, etc.) render transparent (yellowish) gels which cannot be evenly extended on the surface of the glass plates, therefore thwarting the creation of any film by the spinning method.

3.2. Effect of Rotating Speed on the Thickness of SnO_2 Films. Figure 1 shows the thicknesses of SnO_2 xerogel films created from molar ratios $R = 3$ and 4 as function of the rotation frequency.

There, it can be observed that the film thickness becomes thinner as the spinning rate increases; the thicknesses vary in the intervals [150, 77 nm] for $R = 3$ and [152, 131 nm] for $R = 4$, hence with 50 and 14% width diminutions, respectively, taking place. The centrifugal force should be the primary factor that is responsible for such behavior.

However, when the amount of water becomes large (i.e., $R > 4$), the hydrolysis and condensation rates become faster and the viscosity of the gelling system increases accordingly; this viscosity effect counteracts somewhat the thinning effect produced by a larger rotation frequency. The combination of

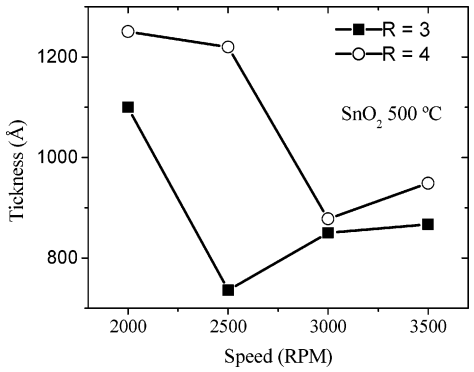

Figure 2. Thickness of Sn xerogel films calcined at 500 °C.

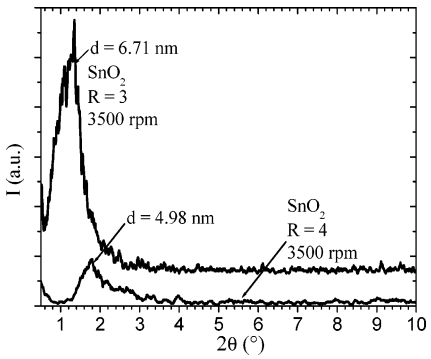

Figure 3. X-ray diffraction patterns of SnO_2 films calcined at 500 °C in air and prepared from $H_2O/Sn(OAm^t)_4$ molar ratios equal to 3 and 4.

the two previous effects explains why the thicknesses of films created with $R = 4$ become thicker than those obtained with $R = 3$.

Figure 2 represents the variation in film thickness with respect to rotation speed for substrates treated at 500 °C for 2 h. First, for $R = 4$, a slight thickness decrease is observed up to 2500 rpm; afterward, a sharp decrease takes place, and finally, the thickness remains more or less stable. This behavior is caused by the combination of several processes. First, the increasing spinning rate is responsible for the slight decrease in film thickness that is initially observed; afterward, evaporation of H_2O causes not only the shrinkage of the gelling film but also the acceleration of the sol−gel transformation reactions. The latter process can bring about the creation of O−Sn−OH bridging species that can interact with the OH groups existing on the glass surface, thus further contracting the adhered film. For $R = 4$, the film thickness decreases sharply from 2500 to 3000 rpm and thereon remains almost stable; once more, the gelling process is speeded up by H_2O evaporation.

3.3. XRD Patterns of SnO_2 Films. The X-ray diffraction patterns of SnO_2 film samples prepared from molar ratios $R = 3$ and 4, at spinning frequencies of 3500 rpm and treated for 2 h at 500 °C in air, are shown in Figure 3. Both diffraction patterns show somewhat distinctive peaks at low diffraction angles, thus seemingly indicating the occurrence of some kind of ordered mesostructure within the samples. It is relevant to stress that thin films proceeding from $R > 4$ render shallow (i.e., unstructuralized) XRD patterns. For $R = 3$, the diffraction angle corresponding to the maximum peak renders an interlayer spacing of 6.71 nm after application of Bragg's law, a value that (as will be shown later) is close to the mode pore size obtained from N_2 sorption studies (i.e., 6.1 nm). For $R = 4$, the highest peak of the XRD pattern indicates a diffraction spacing of about 4.98 nm, that is close to the 4.6−4.9 nm mode pore

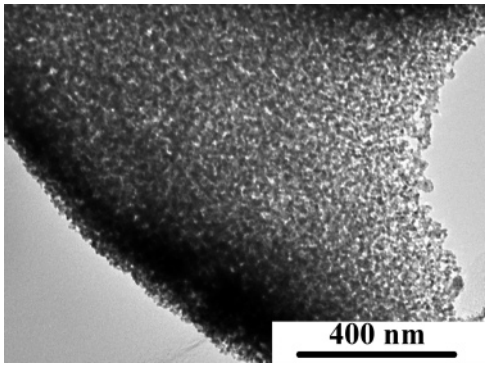

Figure 4. TEM micrograph of film sample $R = 3$ formed at 3500 rpm.

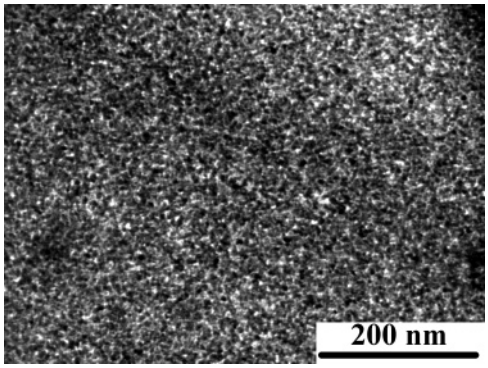

Figure 5. TEM micrograph of film sample $R = 4$ formed at 3500 rpm.

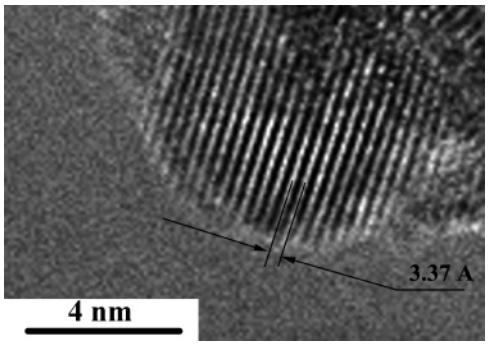

Figure 6. HRTEM micrograph of a SnO_2 film sample created at $R = 3$ and 3500 rpm. SnO_2−cassiterite planes are observed.

size obtained from N_2 sorption. The XRD sizes obtained for $R = 3$ and 4 strongly indicate that our SnO_2 films are mesoporous substrates made of relatively ordered pore arrays. The shorter interlayer spacing observed for $R = 4$ hints the existence of narrower pore templates in this system if compared to those present when $R = 3$.

3.4. TEM of SnO_2 Thin Films. Figures 4−6 display TEM images of films synthesized from preparations involving $R = 3$ and 4. These films were created by depositing a drop of the corresponding Sn sol on a NaCl monocrystal; afterward, this crystal was spun at 3500 rpm to produce the films. It was observed that rotating frequencies smaller than 3500 rpm redound in films too thick to become observable by TEM. Before performing the TEM analysis, the films were annealed at 500 °C in air for 2 h. Subsequently, the SnO_2 films were separated from the NaCl bases by dissolving this salt in distilled water; the films were then deposited on 300 mesh copper grids for TEM observation.

The TEM images in Figures 4 and 5 display pore mouths disseminated along the SnO_2 films proceeding from $R = 3$ and

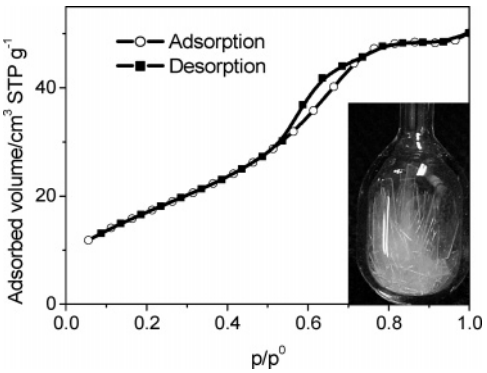

Figure 7. N_2 sorption isotherm on SnO_2 films with $R = 3$ prepared at 3500 rpm and calcined at 500 °C. The inset shows a photograph of the adsorption cell enclosing the glass plates coated with SnO_2 films.

TABLE 2: Textural Parameters of SnO_2 Films Determined by N_2 Sorption

sample	SnO_2, $R = 3$	SnO_2, $R = 4$
A_{BET} ($m^2\ g^{-1}$)	65	112
pore volume ($mm^3\ g^{-1}$)	75	116
AB-NLDFT mean pore size ±1 SD (nm)	5.9 ± 1.3	4.9 ± 0.7
AB-NLDFT mode pore size (nm)	6.1	4.9
DB-NLDFT mean pore width ±1 SD (nm)	6.3 ± 0.5	5 ± 1.1
DB-NLDFT mode pore size (nm)	6.1	4.6

$R = 4$ preparations, respectively. The SnO_2 pore arrangements in these films look somewhat systematic, reasonably monodisperse with regard to size, and evidently mesoporous. The HRTEM micrograph of a SnO_2 thin film (Figure 6) shows an arrangement of parallel layers of this compound due to the partial crystallization of this oxide caused by heat treatment at 500 °C. The interlayer distance of 3.37 Å (Figure 6) is similar to one of the unit cell parameters of the SnO_2−cassiterite phase (3.118 Å).

3.5. N_2 Sorption Characterization of SnO_2 Thin Films. Figure 7 displays the N_2 sorption isotherm at 76 K on a SnO_2 thin film sample synthesized from a sol prepared at $R = 3$; the film was obtained after undergoing a spinning frequency of 3500 rpm over a glass plate, followed by calcination at 500 °C for 2 h.

The isotherm corresponds to a type IV isotherm with an H3 hysteresis loop, with both characteristics being indicative of a mesoporous substrate.[16] The inception point of the hysteresis loop is located at a relative vapor pressure of about 0.55, and an upper plateau is depicted from 0.80 onward. Important structural parameters obtained from the N_2 sorption isotherm are listed in Table 2.

The above isotherm and the values of the textural characteristics suggest the following morphological aspects of SnO_2 films: mesopores are the most abundant voids; neither macropores nor micropores are present in detectable amounts. Macropores can be ruled out because of the existence of an upper isotherm plateau, while micropores are nonexistent because of the aspect of the corresponding *t*-curve[17] (i.e., the latter plot has a negligible ordinate to the origin).

Figure 8 represents the pore-size distribution (PSD) of the SnO_2 film synthesized at $R = 3$. The nonlocal density functional theory[18] (NLDFT) formalism has been employed to determine this PSD curve; cylindrical menisci have been assumed to analyze the adsorption boundary (AB) curve, while spherical interfaces are considered for the desorption boundary (DB) isotherm. The NLDFT-PSD curves calculated from the adsorption and desorption branches of the isotherm are very similar

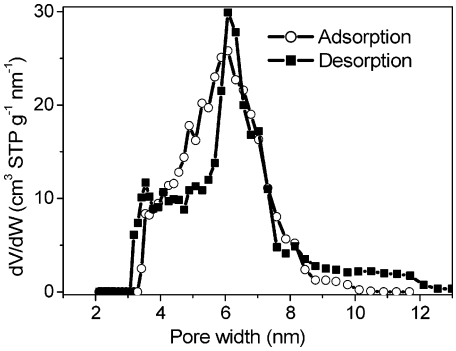

Figure 8. Pore-size distribution of SnO_2 mesoporous films with $R = 3$. W represents the pore width, while V is the adsorbed volume.

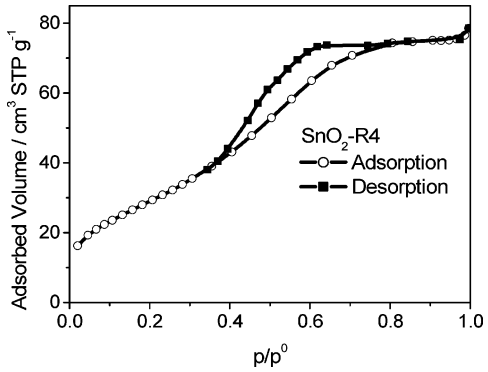

Figure 9. N_2 sorption isotherm on SnO_2 films with $R = 4$ prepared at 3500 rpm and calcined at 500 °C.

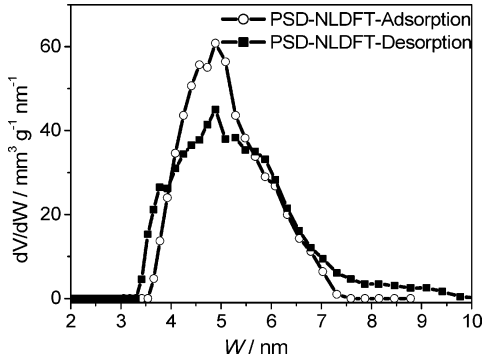

Figure 10. Pore-size distribution of SnO_2 mesoporous films with $R = 4$.

to each other and both show a maximum at about 6.1 nm. These facts are relevant, since they suggest (because of the remarkable coincidence between the adsorption and desorption PSD outcomes) that a cylindrical pore geometry is a very good approximation concerning the shapes of the voids existing in the SnO_2 films. As mentioned before, the mean pore size arising from sorption studies is in good agreement with the Bragg's law XRD result (6.7 nm); the XRD width is larger than the N_2 sorption mean pore size, since it is a center-to-center distance that needs to be corrected by subtraction of the pore wall thickness in order to obtain the actual pore size.

Figure 9 displays the N_2 sorption isotherm of SnO_2 films prepared from $R = 4$ at 3500 rpm. Figure 10 depicts the corresponding NLDFT-PSD of this sample. Once again, the adsorption and desorption PSD curves are practically identical, and maxima occur at about 5 nm.

3.6. Summary Considerations Concerning the Nonsurfactant Synthesis and Textural Properties of SnO_2 Nanofilms. On the basis of the experimental information obtained in the previous sections, we are now able to advance the following hypotheses concerning the surfactantless synthesis of SnO_2 homogeneous thin films. First, we should recognize that two key aspects allow the formation of SnO_2 mesoporous thin films on top of glass substrates by a spinning sol−gel route. The first crucial aspect is a very important one, since, based on experience, the addition of acetylacetone (or some other appropriate chelating compound) to a particular metal alkoxide is unavoidable in order to obtain sols (instead of gels) as precursors for the homogeneous formation of thin films of metal oxides. The inhibiting action of acac on the reactivity of alkoxide molecules prevents (as water is added) excessively high rates of the sol−gel hydrolysis and condensation reactions, thus leading to the attainment of metastable sols, which can later be spread in the form of homogeneous thin films on the surface of glass plates. The second key aspect concerns the selection of convenient values of the water-to-alkoxide molar ratio, since, according to our experience, for the particular case of Sn-$(OAm^t)_4$, this parameter should fall in the range 2−4 in order to generate suitable precursory sols for thin film formation. A molar ratio smaller than 2 delivers negligible amounts of SnO_2, while a value larger than 4 produces gels rather than sols, thus making the spreading of these colloids as thin films on the surface of glass plates somehow impossible.

The present work about thin film formation is one in which it is possible to create a metal oxide mesoporous matrix without needing to simultaneously utilize surfactant molecules, which (during traditional structure-directed syntheses) lead to the formation of precursory micelles that will later reflect their geometrical shape on the resultant mesoporous voids. Thus, what is really happening with our surfactantless mesoporous thin film formation technique? In our opinion, the extra-long aging time (~3 months), allowed by us to the initial sol in order to increase the length and ramification of the oligomer molecules constituting it, has permitted the formation of relatively long and spatially ordered oligomeric molecules. Afterward, as HCl and H_2O are added, the oligomeric species partially lose their stability and form spherical or cylindrical arrangements consisting of a polymerizing shell surrounding a fluid core. The subsequent coacervation of spherical entities, which is mainly caused by surface electrostatic reasons, also renders cylinders (i.e., precursory pore templates) with internal diameters of 5−6 nm. These cylindrical assemblages consist of a polymerizing shell of SnO_2 that encapsulates the remaining nonspent fluid reagents or dissolvents and can be set orderly along their longitudinal axes according to a hexagonal packing. The subsequent thermal treatment of thin sol−gel films spread on glass plates eliminates most fluids and can ultimately render SnO_2 mesoporous membranes made of a regular arrangement of tubular pores of widths around 4.9 ± 0.7 and 5.9 ± 1.3 nm (the attainment of these pore-size ranges certainly depends on the specific water-to-alkoxide ratio that is being employed), such as those observed in this work. The above pore formation process might hopefully provide a general surfactantless technique capable of synthesizing quite a large number of metal oxide mesoporous materials provided with tubular voids in an ordered arrangement for specialty applications.

Now, with respect to the fine coincidence found between the adsorption and desorption NLDFT-PSD curves, it is pertinent to say first that the pore structures of our SnO_2 thin films correspond to channel-like xerogel structures. The pores in these thin film networks appear in the form of tubular paths at which condensation can start occurring at around the narrowest channel sections. Condensation around these narrow regions can then trigger the condensate filling of the whole tube. If these channel-

like pores are not varying too much in cross section, desorption will happen from hemispherical menisci appearing at pore ends and that will have radii of curvature not too different from those arising at the narrow sections at which condensation takes place. The fact of dealing with thin rather than thick films can further contribute to the nice coincidence between the adsorption−desorption PSD curves and justify somehow the control exerted by cylindrical interfaces during capillary condensation and hemispherical menisci throughout capillary evaporation.

Conclusions

A surfactantless method involving the sol−gel processing of tin(IV) tetra-*tert*-amiloxide allows the synthesis of ordered mesoporous SnO_2 thin films. The precursory $Sn(OAm^t)_4$ alkoxide compound should be stabilized with acetylacetone and aged for several months in order to eventually generate oligomeric cylindrical aggregates, which will act as pore templates. The synthesis of appropriate templates for mesoporous thin film formation is finally accomplished when the aged chelated alkoxide is mixed with the proper amount of water (in this case, $H_2O/Sn(OAm^t)_4$ molar ratios equal to 3 or 4 are adequate). The formation of thin films of varying thicknesses on top of glass substrates can be achieved by a spinning procedure performed at rotation speeds between 2000 and 3500 rpm. Films can then be annealed at 500 °C in order to end with mesoporous SnO_2 films deposited on glass surfaces. Application of Bragg's law to the maxima of the XRD patterns results in interlayer distances that are close to the mean pore sizes obtained from N_2 sorption. This fact confirms that the cylindrical aggregates are arranged according to a hexagonal pattern, similar to that existing in SBA-15 substrates.[19] The pore-size distributions calculated from the adsorption and desorption branches of the N_2 sorption isotherms provide practically the same curves. This reconfirms the cylindrical nature of the pores and that cylindrical-like menisci initiate condensation while hemispherical interfaces control the evaporation process. This synthesizing method for producing rather regular mesoporous substrates made of cylindrical pores constitutes a valuable alternative to those methods that involve structure-directing surfactant molecules, for example, SBA-15 or MCM-41 syntheses.

Acknowledgment. We thank Leticia Baños, Luis Rendón, and Patricia Castillo for their assistance in the XRD and TEM experiments. Thanks are also given to CONACYT for the grant awarded to CVO.

References and Notes

(1) Sears, W. M.; Gee, M. A. *Thin Solid Films* **1988**, *165*, 265−277.
(2) Tamura, S.; Ishida, T.; Magara, H.; Mihara, T.; Tabata, O.; Tatsuta, T. *Thin Solid Films* **1999**, *343*−*344*, 142−144**.**
(3) Davazoglou, D. *Thin Solid Films* **1997**, *302*, 204−213.
(4) Leja, E.; Korecki, J.; Toll, K. *Thin Solid Films* **1979**, *59*, 147−155.
(5) He, Y. S.; Campbell, J. C.; Murphy, R. C.; Arendt, M. F.; Swinnea, J. S. *J. Mater. Res.* **1993**, *8*, 12−31.
(6) Strawbridge, I.; Craievich, A. F.; James, P. F. *J. Non-Cryst. Solids* **1985**, *72*, 139−157.
(7) Klein, L. C.; Garvey, G. J. *Mater. Res. Soc. Symp. Proc.* **1984**, *32*, 33.
(8) Glaser, P. M.; Pantano, C. G. *J. Non-Cryst. Solids* **1984**, *63*, 209−221.
(9) Brinker, C. J.; Hurd, A. J.; Schunk, P. R.; Frye, G. C.; Ashley, C. S. *J. Non-Cryst. Solids* **1992**, *147*−*148*, 424−436.
(10) Bradley, D. C.; Holloway, H. *Can. J. Chem.* **1962**, *40*, 1176−1182.
(11) Gulliver, E. A.; Garvey, J. W.; Wark, T. A.; Hampden-Smith, M. J.; Datye, A. K. *J. Am. Ceram. Soc*. **1991**, *74*, 1091−1094.
(12) Chen, F.; Liu, M. *Chem. Commun.* **1999**, 1829−1830.
(13) Velásquez, C. Synthesis, Characterization and Properties of tin (IV) tetra-*tert*-amyloxide $Sn(OAm^t)_4$. M.Sc. Thesis, Universidad Autónoma Metropolitana−Iztapalapa, México, D.F., July 1998.
(14) Thomas, I. M. Stannic tertiary alkoxide. U.S. Patent 3,946,056, March 23, 1976.
(15) Sanchez, C.; Livage, J.; Babonneau, F. *J. Non-Cryst. Solids* **1998**, *100*, 65−76.
(16) Sing, K. S. W.; Everett, D. H.; Haul, R. A. W.; Moscou, L.; Pierotti, R. A.; Rouquerol, J.; Siemieniewska, T. *Pure Appl. Chem.* **1985**, *57*, 603−619.
(17) Gregg, S. J.; Sing, K. S. W. *Adsorption, Surface Area and Porosity*; Academic Press: London, 1982.
(18) Ravikovitch, P. I.; Neimark, A. V. *J. Phys. Chem. B* **2001**, *105*, 6817−6823.
(19) Ojeda, M. L.; Esparza, J. M.; Campero, A.; Cordero, S.; Kornhauser, I.; Rojas, F. *Phys. Chem. Chem. Phys.* **2003**, *5*, 1859−1866.